January 2006

Chaos in Atomic Force Microscopy

Shuiqing Hu
Birck Nanotechnology Center and School of Mechanical Engineering, Purdue University, shuiqing@purdue.edu

Arvind Raman
Birck Nanotechnology Center and School of Mechanical Engineering, Purdue University, raman@purdue.edu

Chaos in Atomic Force Microscopy

Shuiqing Hu and Arvind Raman

Birck Nanotechnology Center and School of Mechanical Engineering, Purdue University, West Lafayette, Indiana 47907, USA

(Received 3 June 2005; published 27 January 2006)

Chaotic oscillations of microcantilever tips in dynamic atomic force microscopy (AFM) are reported and characterized. Systematic experiments performed using a variety of microcantilevers under a wide range of operating conditions indicate that softer AFM microcantilevers bifurcate from periodic to chaotic oscillations near the transition from the noncontact to the tapping regimes. Careful Lyapunov exponent and noise titration calculations of the tip oscillation data confirm their chaotic nature. AFM images taken by scanning the chaotically oscillating tips over the sample show small, but significant metrology errors at the nanoscale due to this ''deterministic'' uncertainty.

DOI: 10.1103/PhysRevLett.96.036107 PACS numbers: 68.35.Ja, 05.45.Tp, 07.79.Lh, 68.37.Ps

Deterministic chaos underpins the dynamics of many nonlinear systems that display a very high degree of sensitivity to initial conditions. In what follows we observe and characterize chaos in the oscillations of nanoscale tips in amplitude modulated atomic force microscopy (AM-AFM). Specifically, we find that chaotic tip dynamics often occur upon the transition from the noncontact to the tapping regimes indicating the presence of complex grazing dynamics. Chaotic dynamics are also observed under conditions of hard tapping. Furthermore, we show that the presence of chaos can lead to errors while imaging samples using dynamic AFM, thereby introducing an element of deterministic uncertainty in nanometrology.

In dynamic AFM [1], a micromechanical oscillator, a silicon microcantilever with an attached nanoscale tip, is driven near the oscillator resonance frequency in the close vicinity of the sample surface. During each oscillation cycle the nanoscale tip can experience a variety of short and long range forces between the tip and the sample such as [2] electrostatic, van der Waals, capillary, specific chemical, Pauli repulsion, and nanoscale contact and elastic forces. These interaction forces are highly nonlinear, and consequently it is possible that the oscillating tip exhibits chaotic spectra that contain a wide range of constituent frequencies. Because tip oscillations at frequencies other than the driving frequency are not controlled in AM-AFM [3,4], chaotic tip oscillation spectra can lead to fundamental and important errors in both the metrology and the force spectroscopy of the scanned sample.

Prior to the present work, both Burnham *et al.* [5] and Salapaka *et al.* [6] have reported complicated microcantilever dynamics in experiments where vibrating samples were made to impact a stationary microcantilever. The present work deals more directly with nanoscale imaging and spectroscopy in dynamic AFM where the microcantilever is driven near its fundamental resonance.

The experimental setup consists of a Picoplus™ AFM system, together with an external Signal Recovery™ lock-in amplifier, and a data acquisition system based on National Instruments 5911 boards. To minimize the effects of water meniscus, the experiments are performed under dry nitrogen environment on the hydrophobic surface of freshly cleaved highly ordered pyrolytic graphite (HOPG) supplied by SPI Supplies™. For comparison, the same sets of experiments are also performed under ambient conditions. The experiments are performed with three different sets of microcantilevers, each set consisting of approximately ten microcantilevers with properties that are shown in Table I. This represents a wide range of microcantilever bending stiffnesses and fundamental resonance frequencies (ω_0).

The goal of the experimental procedure is to demonstrate the existence of chaos and its effects on nanometrology within the context of AM-AFM. Accordingly, for each microcantilever, the tip amplitude at the driving frequency (*setpoint amplitude*) is maintained constant via the lock-in amplifier and the AFM control system. The driving amplitude of the dither piezo is gradually increased in increments of 0.49 nm by increasing the voltage supplied to the dither piezo; this effectively decreases the *setpoint amplitude ratio.* At each driving voltage, both the tip oscillation and the piezo excitation signal are recorded. These experiments are performed for two setpoint amplitudes [7], namely, 80 and 140 nm. Moreover, these experiments are performed for cases when the driving frequency $\Omega = 0.98\omega_0$, $\Omega = \omega_0$, and $\Omega = 1.02\omega_0$. Finally, each experiment was repeated 6 times to verify the repeatability of the results. The observed phenomena are robust over the six repeats of each experiment, and also consistent between the approximately ten microcantilevers tested within each set. Put together, this represents a substantial body of experimental data [8] representing dynamic AFM under a wide range of operating conditions and using a wide variety of microcantilevers.

A summary of all the experimental results may be found in Table I; however, in this Letter we focus our attention on experiments performed under dry nitrogen using the set of Nanosensor™ Force Modulation silicon microcantilevers ($\omega_0 \sim 66.3$ kHz) when $\Omega = \omega_0$ and with a setpoint amplitude of 80 nm. The phenomena observed in this set of microcantilevers under these operating conditions span the phenomena observed for all other sets of microcantilevers. In what follows we analyze the time series tip oscillation

TABLE I. Properties and observed transitions of oscillation states for 3 sets of microcantilevers (the stiffness, resonance frequency, and quality factor are ascertained from experimental data and are averaged over the 10 microcantilevers within each set) as the driving amplitude is gradually increased. The onset of chaos is determined by calculating the noise limit and Lyapunov exponents of the tip oscillation data. The symbol $\hat{\rightarrow}$ indicates a simultaneous transition from the noncontact to the tapping regime.

Cantilever set			Force modulation	Ultrasharp NSC12-C	TESP
Fundamental resonance frequency (kHz)			63.3 ± 2.1	130.2 ± 1.8	310.1 ± 5.9
Stiffness (N/m)			1.5 ± 0.1	2.9 ± 0.2	148 ± 5
Quality factor			142 ± 8	130 ± 11	148 ± 5
Transitions under nitrogen	Setpoint amplitude = 80 nm	$\Omega = 0.98\omega_0$,	Period-1 $\hat{\rightarrow}$ period-2 $\rightarrow$ period-4	Period-1 $\hat{\rightarrow}$ chaotic	Period-1 $\hat{\rightarrow}$ period-1
		$\Omega = \omega_0$,	Period-1 $\hat{\rightarrow}$ chaotic $\rightarrow$ period-2 $\rightarrow$ chaotic	Period-1 $\hat{\rightarrow}$ chaotic	Period-1 $\hat{\rightarrow}$ period-1
		$\Omega = 1.02\omega_0$,	Period-1 $\hat{\rightarrow}$ chaotic	Period-1 $\hat{\rightarrow}$ chaotic	Period-1 $\hat{\rightarrow}$ period-1
	Setpoint amplitude = 140 nm	$\Omega = 0.98\omega_0$,	Period-1 $\hat{\rightarrow}$ period-2 $\rightarrow$ period-4	Period-1 $\hat{\rightarrow}$ period-1	Period-1 $\hat{\rightarrow}$ period-1
		$\Omega = \omega_0$,	Period-1 $\hat{\rightarrow}$ chaotic $\rightarrow$ period-1 $\rightarrow$ period-2	Period-1 $\hat{\rightarrow}$ period-1	Period-1 $\hat{\rightarrow}$ period-1
		$\Omega = 1.02\omega_0$,	Period-1 $\hat{\rightarrow}$ chaotic	Period-1 $\hat{\rightarrow}$ period-1	Period-1 $\hat{\rightarrow}$ period-1
Transitions in air	Setpoint amplitude = 80 nm	$\Omega = 0.98\omega_0$,	Period-1 $\hat{\rightarrow}$ period-2 $\rightarrow$ period-4	Period-1 $\hat{\rightarrow}$ chaotic	Period-1 $\hat{\rightarrow}$ period-1
		$\Omega = \omega_0$,	Period-1 $\hat{\rightarrow}$ chaotic $\rightarrow$ period-1 $\rightarrow$ chaotic	Period-1 $\hat{\rightarrow}$ chaotic	Period-1 $\hat{\rightarrow}$ period-1
		$\Omega = 1.02\omega_0$,	Period-1 $\hat{\rightarrow}$ chaotic	Period-1 $\hat{\rightarrow}$ chaotic	Period-1 $\hat{\rightarrow}$ period-1
	Setpoint amplitude = 140 nm	$\Omega = 0.98\omega_0$,	Period-1 $\hat{\rightarrow}$ period-2 $\rightarrow$ period-4	Period-1 $\hat{\rightarrow}$ period-1	Period-1 $\hat{\rightarrow}$ period-1
		$\Omega = \omega_0$,	Period-1 $\hat{\rightarrow}$ period-2 $\rightarrow$ period-1 $\rightarrow$ chaotic	Period-1 $\hat{\rightarrow}$ period-1	Period-1 $\hat{\rightarrow}$ period-1
		$\Omega = 1.02\omega_0$,	Period-1 $\hat{\rightarrow}$ chaotic	Period-1 $\hat{\rightarrow}$ period-1	Period-1 $\hat{\rightarrow}$ period-1

data acquired for this set of microcantilevers under the above conditions at each driving voltage.

In order to detect rigorously the presence of chaos in the tip oscillation time series data at each driving amplitude, we use two different time series analysis methods—(a) calculation of the largest Lyapunov exponent, and (b) calculation of the noise limit of titration of chaos. The Lyapunov exponents λ_i, $i = 1, \ldots, N$ are the averaged rates of divergence (or convergence) of two neighboring trajectories in phase space. The number of Lyapunov exponents N equals the dimension of the phase space, and a positive Lyapunov exponent is indicative of chaos. We use the "lyp_k" routine of TISEAN 2.1 a nonlinear time series analysis package [9] to estimate the largest Lyapunov exponent of the tip oscillation data at each driving amplitude. Because the Lyapunov exponent may be an erroneous indicator of chaos in the presence of noise [10], we also use titration of chaos with added noise [11], a relatively new method that can robustly detect chaos with short noisy experimental data. Specifically this method detects the nonlinearity in a time series by comparing short time prediction results of nonlinear and linear Volterra-Wiener-Korenberg series. White noise of increasing standard deviation is added to the chaotic time series until its nonlinearity cannot be detected by a particular numerical indicator. We denote this value of the noise limit (NL) as the "noise ceiling" of the signals corresponding to the amount of chaos. NL > 0 indicates chaos; NL $= 0$ indicates that the data series either is not chaotic or the chaotic component is already neutralized by the background noise in the original time series. The results for the Lyapunov exponents and the NL (calculated using a previously published algorithm [12]) are shown in Fig. 1. Clearly both the titration of the chaos method and the Lyapunov exponent method yield the same results and confirm that chaotic oscillations set in at the transition from the noncontact to the tapping regime of oscillation (at 37.2% setpoint amplitude ratio) and then again under hard tapping conditions. The presence of the noncontact to tapping transition is confirmed by measuring the phase of the oscillation [13]. Following the transition from noncontact to tapping, the tip continues to oscillate chaotically for driving amplitudes between 1.23 and 2.70 nm, then suddenly transitions to a period-2 oscillation and becomes chaotic again when the driving amplitude is larger than 4.66 nm.

We now explore the consequences of imaging the freshly cleaved atomically flat HOPG surface in different regimes [14]. For the driving amplitude 0.49 nm the tip is in a period-1 [15] oscillation state, in the noncontact regime. The tip vibration power spectral density shows superharmonics, but the tip motion is still period-1 as shown in the

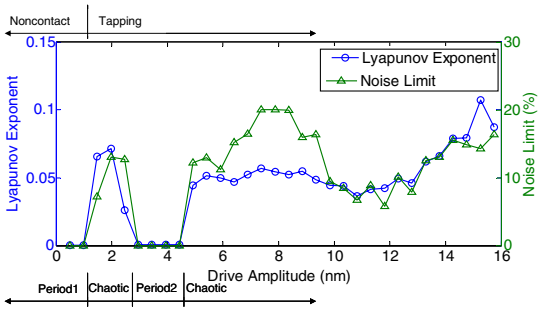

FIG. 1 (color online). Largest Lyapunov exponent and noise limit versus dither piezo driving amplitude for one of the Force Modulation ($\omega_0 = 66.3$ kHz) microcantilevers in a dry nitrogen environment over freshly cleaved HOPG.

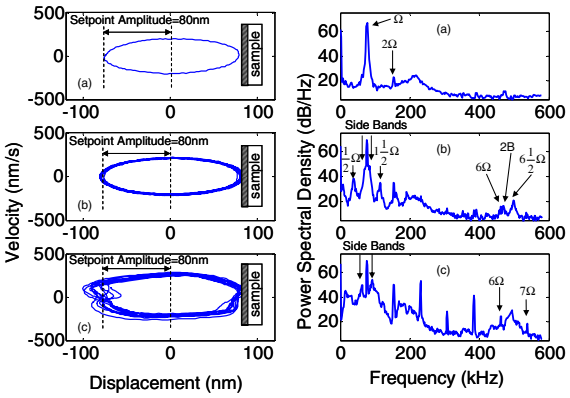

FIG. 2 (color online). Tip deflection phase portrait (left) and power spectral density (right) versus dither piezo drive amplitude of (a) 0.49 nm (period-1, noncontact regime), (b) 1.97 nm (chaotic, tapping regime), and (c) 14.76 nm (chaotic, tapping regime). The vertical line in the phase portrait represents the position of the sample surface. Ω denotes the driving frequency, and 2B denotes the second bending mode frequency of the microcantilever. In the phase portrait, the tip velocity is computed by differentiating the experimental tip vibration signal using moving averages.

phase portrait plot in Fig. 2(a). Figure 3(a) shows the topology map of the freshly cleaved HOPG surface and the map of the error signal (the difference between the setpoint amplitude and the actual amplitude of the tip at the driving frequency) acquired under these conditions. Imaging the sample in this regime produces accurate topology images of freshly cleaved HOPG, and the error is nearly zero everywhere except at the edges of the HOPG layers. Figure 2(b) shows tip deflection phase portrait and power spectral density at the drive amplitude of 1.97 nm when the tip is in its first chaotic oscillation state at the

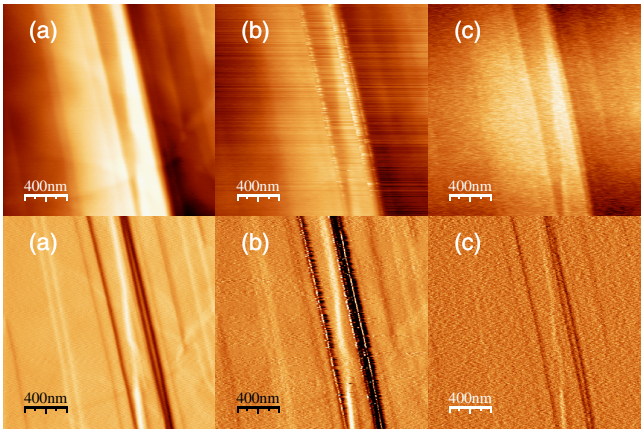

FIG. 3 (color online). Influence of chaotic tip oscillations on the nanometrology of a freshly cleaved HOPG surface. Topology map (top) and error map (bottom) with driving amplitudes of (a) 0.49 nm (period-1, noncontact regime), (b) 1.97 nm (chaotic, tapping regime), and (c) 14.76 nm (chaotic, tapping regime). The scan area is $2 \times 2\ \mu\text{m}^2$.

transition from the noncontact to the tapping regime. The spectrum now contains superharmonics, subharmonics, and side bands, and the noise floor increases as seen in the power spectrum. A significant sixth harmonic of the driving frequency also appears in the tapping regime near the second bending mode resonance frequency [denoted by "2B" in Fig. 2(b)]. This is attributed to a nonlinear coupling between two different modes of the continuous microcantilever beam—the fundamental mode and the second bending mode whose resonance frequency is close to 6 times that of the fundamental. This condition is also referred to as a 1:6 internal resonance [16]. Figure 3(b) shows the topology map and the error map at a driving amplitude of 1.97 nm. Clearly the error map is noisy even on the atomically flat part of the HOPG sample due to the chaotic nature of the tip oscillation. Finally, when the driving amplitude is at 14.76 nm and the tip is in the second chaotic oscillation state in the hard tapping regime, the phase portrait indicates chaotic dynamics and the spectrum becomes broadband as shown in Fig. 2(c). Both the topology and the error map in Fig. 3(c) are extremely noisy. We conclude that the presence of chaotic tip oscillations deteriorates noticeably the ability of AM-AFM to perform high precision nanometrology.

The noise titration and Lyapunov exponent calculations were performed for each experiment for every cantilever under different operating conditions. In all cases both calculations yield the same results. The results of observed dynamics are summarized in Table I. Except for very stiff and high frequency microcantilevers [such as the set of tapping mode etched silicon probe (TESP) microcantilevers, $\omega_0 \sim 310$ kHz], all other microcantilevers tested undergo chaotic oscillations upon transition from the noncontact to the tapping regimes for certain operating parameters.

These experimental results provide compelling evidence for the underlying mechanism of chaos in this nanoscale dynamical system. Specifically the observed sequence of bifurcations in Table I is predicted by the global dynamics of the two-dimensional Nordmark map, which is often used to model single degree-of-freedom nonsmooth systems. For instance, two bifurcations of grazing trajectories are commonly observed [17,18] in the Nordmark map. One is from a stable period-1 orbit to a chaotic attractor at the gazing incidence; another is when a stable period-1 orbit connects to a stable period-M maximal orbit through an unstable period-M orbit via a saddle node bifurcation. These two bifurcations are very similar to the bifurcations "period-1 $\rightarrow$ chaotic" and "period-1 $\rightarrow$ period-2 $\rightarrow$ period-1" observed in our experiments at the transition from the noncontact to the tapping regime (as shown in Table I). In spite of their similarities, several aspects of the experimental results cannot be fully captured by the predictions of the Nordmark map. For instance, the experimental results clearly indicate a 1:6 internal resonance [16] between the first and second bending modes. We anticipate

therefore that the full range of our experimental results is likely to be adequately captured in a higher dimensional equivalent of the two-dimensional Nordmark map. Finally, we note that another mechanism of chaos, namely, homoclinic chaos has been investigated in theoretical AFM dynamics models [19,20]. However, this requires the cantilever to be placed very close to the sample surface (<5 nm). We have not investigated in this regime because this is a relatively rare situation in AM-AFM where the cantilever is kept at least 10 nm away from the sample, typically 25–150 nm.

It is interesting to speculate on the fundamental physical mechanisms in our experiments that could lead to effectively nonsmooth interaction forces. While the formation and breaking of nanoscale liquid necks between the tip and the sample could lead to such effects, the experimental conditions minimize this effect. Instead, when the tip comes very close to the sample, it is known from molecular dynamics simulations [21] that instabilities occur between the atoms at the very end of the tip and the atoms at the sample surface. These instabilities occur at time scales that are extremely small compared to the time scale of tip oscillations and could lead to effectively nonsmooth tip-sample interaction forces.

Several key conclusions can be drawn from the above results. First, the frequent onset of chaotic dynamics at the transition from the noncontact to the tapping regimes indicates the presence of complex grazing bifurcations such as those predicted in the Nordmark map. This is an important observation because the transition from the noncontact to the tapping regime often occurs under realistic operating conditions used for AFM imaging. Second, stiff cantilevers seem immune to chaotic dynamics under the operating conditions tested in this work; however, they also generate larger tip-sample interaction forces. Finally, in the chaotic spectra of the microcantilevers (such as for the 66.3 kHz microcantilever discussed at length) more than 80% of the vibration energy is still concentrated at the driving frequency. The observed chaos is ''weak'' in this sense because it contains a strong periodic component.

In conclusion, we have observed and characterized thoroughly and repeatably the onset of weak chaos in microcantilevers with nanoscale tips tapping on HOPG under a variety of operating conditions. We have also demonstrated that the presence of chaos deteriorates the image quality and introduces deterministic uncertainty in nanometrology. These metrology errors are expected to be small for most current applications; however, as nanometrology requirements become increasingly stringent, the presence of chaos is likely to pose some fundamental deterministic limits on measurement resolution.

Financial support of this research by the National Science Foundation (NSF) under Contracts No. 0116414-CMS and No. 0409660-CMS is gratefully acknowledged. We also thank Professor R. Reifenberger (Condensed Matter Physics, Purdue University) for helpful discussions.

[1] R. García and R. Pérez, Surf. Sci. Rep. **47**, 197 (2002).
[2] J. N. Israelachvili, *Intermolecular and Surface Forces* (Academic Press, San Diego, 1992), 2nd ed.
[3] M. Stark *et al.*, Proc. Natl. Acad. Sci. U.S.A. **99**, 8473 (2002).
[4] R. W. Stark, G. Schitter, M. Stark, R. Guckenberger, and A. Stemmer, Phys. Rev. B **69**, 085412 (2004).
[5] N. A. Burnham, A. J. Kulik, G. Gremaud, and G. A. D. Briggs, Phys. Rev. Lett. **74**, 5092 (1995).
[6] S. Salapaka, M. Dahleh, and I. Mezić, Nonlinear Dyn. **24**, 333 (2001).
[7] We use the Z piezotube controller to maintain the setpoint amplitude in the presence of thermal drifts. However, during the data acquisition this controller is turned off. The Z piezotube controller therefore effectively resets the gap to the approximate setpoint amplitude preceding each increment in driving amplitude. Note that since only the setpoint amplitude is maintained constant, other frequency components are uncontrolled, and the gap between the cantilever and sample will still vary a little at different driving amplitudes.
[8] The lock-in amplifier triggers the 5911 boards to initiate the data acquisition. The lock-in amplifier and AFM controller are fully controlled by VISUAL BASIC script programs. In this manner, the entire experiment sequence with a specific microcantilever is performed automatically with one program.
[9] H. Kantz and T. Schreiber, *Nonlinear Time Series Analysis* (Cambridge University Press, Cambridge, 1997).
[10] L. Arnold, P. Imkeller, and N. S. Namachchivaya, J. Sound Vib. **269**, 1003 (2004).
[11] M. Barahona and C. Poon, Nature (London) **381**, 215 (1996).
[12] C. Poon and M. Barahona, Proc. Natl. Acad. Sci. U.S.A. **98**, 7107 (2001).
[13] R. García and A. San Paulo, Phys. Rev. B **61**, R13 381 (2000).
[14] For a fair comparison, the imaging feedback control parameters for these three cases are identical, so that any differences in imaging quality are entirely due to the tip oscillation state. Also optimizing control parameters does not further improve the imaging quality.
[15] A period-n motion is a periodic motion with a fundamental period that is $1/n$ of the excitation signal.
[16] A. H. Nayfeh, *Nonlinear Interactions: Analytical, Computational, and Experimental Methods* (Wiley-Interscience, New York, 2000).
[17] W. Chin, E. Ott, H. E. Nusse, and C. Grebogi, Phys. Rev. E **50**, 4427 (1994).
[18] F. Casas, W. Chin, C. Grebogi, and E. Ott, Phys. Rev. E **53**, 134 (1996).
[19] M. Basso, L. Giarré, M. Dahleh, and I. Mezić, Trans. ASME: J. Dyn. Syst. Meas. Control **122**, 240 (2000).
[20] A. Ashhab, M. Salapaka, M. Dahleh, and I. Mezić, Nonlinear Dynamics **20**, 197 (1999).
[21] U. Landman and W. D. Luedtke, J. Vac. Sci. Technol. B **9**, 414 (1991).